Comput Mech (2012) 50:159–168
DOI 10.1007/s00466-012-0733-7

ORIGINAL PAPER

Phase-field modeling of thermomechanical damage in tungsten under severe plasma transients

Tamer Crosby · Nasr Ghoniem

Received: 26 March 2012 / Accepted: 5 May 2012 / Published online: 1 June 2012

Abstract Tungsten is now a primary candidate for plasma facing components in fusion energy systems because of its numerous superior thermophysical properties. International efforts are currently focused on the development of tungsten surfaces that can intercept ionized plasma and pulsed high heat flux in magnetic fusion confinement devices. Thermal shock under transient operating conditions, such as edge localized modes, have experimentally been shown to lead to severe surface and sub-surface damage. We present here a computational multiphysics model to determine the relationship between the thermomechanical loading conditions and the onset of damage and failure of tungsten surfaces. The model is based on thermo-elasto-plasticity constitutive relations, and is developed within the framework of the phase-field method. A coupled set of partial differential equations is solved for the temperature, displacement, and a damage phase fields under severe plasma transient loads. The results clearly show the initiation and propagation of surface and sub-surface cracks as a result of the transient high heat flux. The severity of surface cracking is found to correlate primarily with the magnitude of the near-surface temperature gradient.

Keywords Tungsten · Phase-field modeling · Thermomechanics · Damage mechanics

T. Crosby (✉) · N. Ghoniem
Department of Mechanical & Aerospace Engineering,
University of California at Los Angeles (UCLA), 420 Westwood Plaza,
Los Angeles, CA 90095-1597, USA
e-mail: tcrosby@ucla.edu

N. Ghoniem
e-mail: ghoniem@ucla.edu

1 Introduction

Divertors in fusion reactors are subjected to transient plasma events characterized by high thermal energy for short durations. Edge localized modes, or ELMs for short, are plasma events that result from disruption of the normal operation of current fusion energy devices. These events are expected to be present in devices that are under construction, such as the International Thermonuclear Experimental Reactor (ITER), that is being built in France. ELMs are highly nonlinear magnetohydrodynamic events that are accompanied by high thermal energy (3–10 % of the core thermal energy). Typical surface energy densities in each event fall between 0.1 and 0.5 MJ/m^2 for the Joint European Torus and between 1 and 5 MJ/m^2 for the ITER [12]. The duration of these events is relatively short, usually between 0.1 and 1 ms. Several recent experiments, e.g. [2,11,17], have shown that the damage in the surface region and inside the tungsten material is largely controlled by the severity of plasma or high heat flux transients. This thermomechanical damage may lead to the degradation of the thermophysical properties of tungsten.

Tungsten is also used extensively in many space electric propulsion applications, such as in hollow cathodes in ion and Hall thrusters, or in acceleration grids, where the operating temperature is around 1,453 K [5]. Intermittent operation of space electric propulsion systems induce severe thermomechanical loading conditions as a result of plasma ion bombardment, that can lead to progressive damage accumulation in cathodes or acceleration grids.

The objective of this work is to develop a multiphysics computational model and a modeling tool that is capable of simulating the damage in tungsten surface, manifested by cracks, under severe transient heating conditions similar to those expected in fusion energy and space electric propulsion systems. The multiphysics model, which has new and

unique features of combining a phase-field formulation with elastoplasticity and transient heat conduction is presented next. In Sect. 3, we study the case of a heat load of 1 MJ/m^2 in order to assess the model. In Sect. 4, we implement the formulation on a two-dimensional polycrystalline tungsten, where we study two different heat loads of 1 and 0.1 MJ/m^2. Finally, in Sect. 5 we give our conclusions and final remarks.

2 Phase-field method

Recently, the phase-field methodology has been extended and applied to studies of fracture phenomena as an alternative to detailed front tracking of fractured solids. Such approach has the natural attractiveness of describing the evolution of a "field" quantity representing fracture damage, which can be incorporated in other field descriptions of interacting phenomena. Thus, it provides a powerful and flexible framework for studies of complex fracture damage evolution in materials subjected to arbitrarily complex mechanical or thermal loading. Examples of the use of the phase-field method (PFM) in fracture problems can be found in literature, for example in [3,9,10,13,16]. The general idea of phase-field modeling is to introduce an additional field variable (an order parameter ϕ) that describes the state of the system. This parameter takes the values of 0 and 1, which corresponds to fractured and un-fractured states, respectively. Thus, the parameter can be regarded as a "material continuity" field. The key issue in phase-field problems is the formulation of a free energy functional of the system, which by means of variational principles, results in partial differential equations that are used to calculate the system variables, including the phase-field parameter. A general form of the free energy that may represents many physical systems is [15]:

$$E[\phi,\ T] = \int_V \left\{ \frac{1}{2}|W_o \nabla\phi|^2 + f(\phi(\mathbf{x}),\ T(\mathbf{x})) \right\} \mathrm{d}V \tag{1}$$

The previous equation is referred to as the Ginzburg–Landau or the Cahn–Hilliard free energy, and it serves as the starting point for the modeling of different phenomena using the PFM [15].

Here, we start with an energy functional formulation similar to [10], namely:

$$E\left\{\phi(\mathbf{x}),\ \mathbf{u}(\mathbf{x})\right\} = \int_\Omega \left\{ \frac{1}{2}(\phi^2+\eta)\boldsymbol{\epsilon}(\mathbf{u}) :\ [\boldsymbol{C}\boldsymbol{\epsilon}(\mathbf{u})] + \gamma_c \left(\varepsilon|\nabla\phi|^2 + \frac{(1-\phi)^2}{4\varepsilon} \right) \right\} \mathrm{d}\Omega \tag{2}$$

where ε (mm) and γ_c (N/mm) are the width of the process zone and the fracture surface energy, respectively. $\mathbf{u}$ (mm), $\boldsymbol{\epsilon}$, and $\boldsymbol{C}$ (N/mm^2), are the displacement, strain and elastic moduli, respectively. The first term in the energy functional represents the elastic energy of the system. However, to account for the loss of material when a crack occurs, the elastic energy is multiplied by a degradation term, $(\phi^2+\eta)$, where η is a residual stiffness term, to simulate the energy of fractured areas that has ϕ equals to 0. The second term in the energy equation represents the surface energy of a crack. In the following paragraphs, we extend this model by including two critical aspects of damage physics, which are the thermal field and residual stresses induced by plasticity.

In this work, we are interested in the effects of thermal heat transients on material damage. The previous energy functional must then be modified to include thermal loads. In order to determine the values of residual stresses in the material, plasticity must also be included in the phase-field formulation. First, the strain energy is expressed as:

$$e = \int_\epsilon \sigma_{ij}\mathrm{d}\epsilon^e_{ij} = C_{ijkl}\int_\epsilon \epsilon^e_{kl}\mathrm{d}\epsilon^e_{ij} = \frac{1}{2}C_{ijkl}\epsilon^e_{kl}\epsilon^e_{ij} \tag{3}$$

$$= \frac{1}{2}C_{ijkl}(\epsilon_{kl} - \epsilon^p_{kl} - \alpha T\delta_{kl})(\epsilon_{ij} - \epsilon^p_{ij} - \alpha T\delta_{ij}) \tag{4}$$

where $\boldsymbol{\epsilon}$, $\boldsymbol{\epsilon}^p$, and $\boldsymbol{\epsilon}^e$ are the total, plastic, and elastic strains, respectively. T is the temperature and α is the coefficient of thermal expansion. Here, we used the assumption of small strains, so that the additive decomposition of the total strain into elastic and plastic parts is allowed. For isotropic materials, the elastic stiffness tensor can be expressed in terms of the Lamé constants, λ and μ, as:

$$C_{ijkl} = \lambda\delta_{ij}\delta_{kl} + \mu(\delta_{ik}\delta_{jl} + \delta_{il}\delta_{jk}) \tag{5}$$

the full form of the strain energy, in the two-dimensional case, becomes:

$$e = \frac{\lambda}{2}(\epsilon^2_{ii} + \epsilon^{p\,2}_{ii}) + \mu(\epsilon_{ij}\epsilon_{ij} + \epsilon^p_{ij}\epsilon^p_{ij}) - (\lambda+2\mu)\epsilon_{ij}\epsilon^p_{ij} + 2(\lambda+\mu)\alpha T\left(\alpha T - (\epsilon_{ii} - \epsilon^p_{ii})\right) \tag{6}$$

and the total free energy of the system is:

$$E\left\{\phi(\mathbf{x}),\ \mathbf{u}(\mathbf{x}),\ \boldsymbol{\epsilon}^p(\mathbf{x}),\ T(\mathbf{x})\right\} = \int_\Omega \psi\left(\phi,\ \mathbf{u},\ \boldsymbol{\epsilon}^p,\ T\right)\mathrm{d}\Omega \tag{7}$$

with the energy density expressed as:

$$\psi\left\{\phi(\mathbf{x}),\ \mathbf{u}(\mathbf{x}),\ \boldsymbol{\epsilon}^p(\mathbf{x}),\ T(\mathbf{x})\right\} = \frac{1}{2}(\phi^2+\eta)e(\mathbf{u},\ \boldsymbol{\epsilon}^p,\ T) + \gamma_c\left(\frac{(1-\phi)^2}{4\epsilon} + \epsilon|\nabla\phi|^2\right) \tag{8}$$

By means of variational principles, evolution and equilibrium equations for the field variables are obtained as follows:

$$\frac{\delta\psi}{\delta\phi} = -2\epsilon\gamma_c\nabla^2\phi + \phi e(\mathbf{u},\ \boldsymbol{\epsilon}^p,\ T) + \frac{\gamma_c}{2\epsilon}(\phi - 1)$$
$$= -\frac{\dot{\phi}}{M} \tag{9}$$
$$\frac{\delta\psi}{\delta\mathbf{u}} = (\lambda+\mu)[(\phi^2+\eta)u_{j,j}]_{,i} + \mu[(\phi^2+\eta)u_{i,j}]_{,j} \tag{10}$$
$$-\alpha(\lambda+\mu)[(\phi^2+\eta)T]_{,i}$$
$$+(\lambda+2\mu)[(\phi^2+\eta)\epsilon^p_{ij}]_{,j} = 0 \tag{11}$$
$$\frac{\delta\psi}{\delta T} = (\lambda+\mu)\alpha(\alpha^2+\eta)[2\alpha T - u_{i,i}] = 0 \tag{12}$$

where M (m^2/(N s)) is the mobility. Equation (9) is based on Langevin dynamics, and it acts as an evolution equation for the phase-field parameter ϕ. The next equation is similar to the familiar Navier's equation for equilibrium in linear elasticity, except that it has the thermal and plastic contributions acting as a body force. Also, it has the degradation term $(\phi^2+\eta)$, which acts as a modified constitutive parameter and accounts for fracture. The last equation states that thermal expansion is equal to the volumetric strain, and this has to be satisfied by the solution.

Since the plastic strain is now an additional internal variable, a constitutive equation has to be added to the previous formulation. Here, we use the Prandtl–Reuss incremental plasticity formulation which states [8]:

$$\mathrm{d}\epsilon^p_{ij} = S_{ij}\mathrm{d}\lambda \tag{13}$$

where S_{ij} and σ_m are the deviatoric and mean stresses, respectively, and are defined as:

$$S_{ij} = \sigma_{ij} - \delta_{ij}\sigma_m, \quad \sigma_m = \frac{1}{2}(\sigma_1+\sigma_2) \tag{14}$$

$\mathrm{d}\lambda$ can be obtained by assuming strain hardening:

$$\mathrm{d}\lambda = \frac{3}{2}\frac{\mathrm{d}\sigma_e}{H\sigma_e} \tag{15}$$

thus, the plastic strain increments are now calculated from:

$$\mathrm{d}\epsilon^p_{ij} = \frac{3}{2}\frac{\mathrm{d}\sigma_e}{H\sigma_e}S_{ij} \tag{16}$$

where H is the slope of the hardening curve, and σ_e is the effective stress defined as:

$$\sigma_e = \sqrt{\sigma_1^2 - \sigma_1\sigma_2 + \sigma_2^2} \tag{17}$$

where $\sigma_{1,2}$ are the principle stresses.

3 Benchmarking: a single surface crack

Before proceeding to the polycrystalline case, the previous formulation was implemented on a two-dimensional (0.16 mm × 0.4 mm) slap with an initial single crack and with no nucleation allowed in order to benchmark the model. In this preliminary study, we study the case of a heat flux of 0.2 GW/m^2 applied for 5 ms, so that the total heat load is 1 MJ/m^2. Initially, ϕ was set to 1 everywhere in the material, except on the crack where it was set to 0. The thermal boundary conditions were as follows: a heat flux applied on the left boundary, and a fixed temperature of 450 K was assigned to the right boundary. An infinite element was attached to the original geometry in order to simulate semi-infinite medium, and eliminate boundary effects, just for heat conduction purposes. The mechanical boundary conditions were set free everywhere except on the right boundary where they were fixed. This way, the only forces acting on the material are coming from the applied heat load. In order to understand the role played by different parameters in the model, three parametric studies were conducted where we changed the values of ε, γ_c, and M, one at a time, and looked at the values of ϕ. The results of the parametric studies are shown in Figs. 1, 2, and 3. In the final simulation, the values of some of the

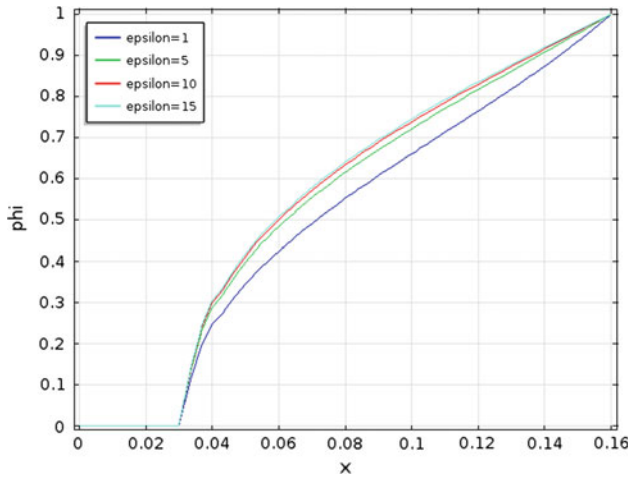

Fig. 1 ϕ versus ε (m)

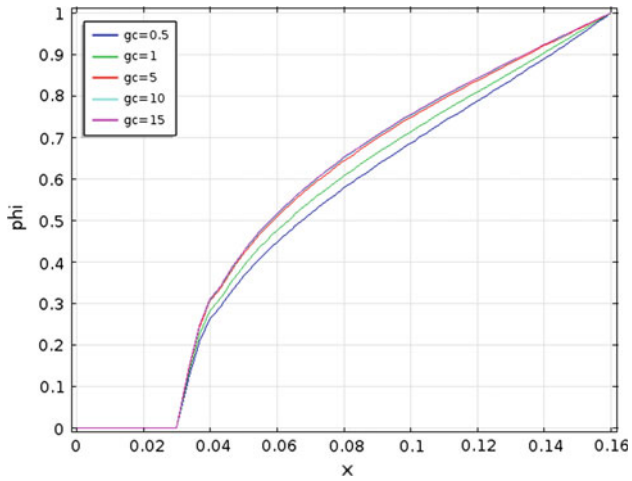

Fig. 2 ϕ versus γ_c (N/m)

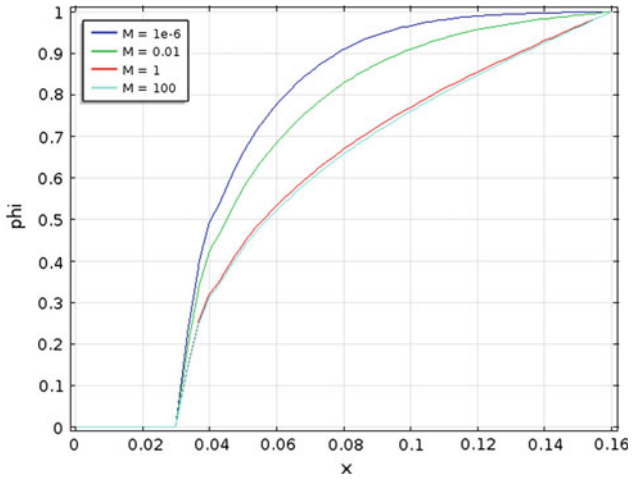

Fig. 3 ϕ versus M ($m^2/(N\,s)$)

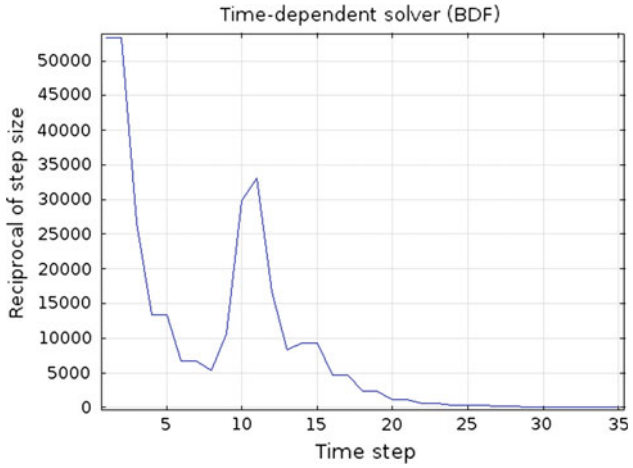

Fig. 4 Convergence of the solution using the time dependent solver

parameters that we used were as follows: $M = 50\,mm^2/(N\,s)$, $\eta = 10^{-5}$, $\varepsilon = 1\,m$.

The model was solved within the framework of the finite element method with the total simulation time set to 0.1 s and the time steps to 0.1 ms. Two types of meshes are used, the first one consists of quadrilateral elements distributed using a free mesh method, and the second one consists of edge elements distributed using the boundary element method. The total number of mesh elements is 6,807 element, with an average element quality of 0.3244 (the quality of an element is a value between 0 and 1, where 0.0 represents a degenerated element and 1.0 represents a completely symmetric element). The time dependent solver used segregated steps that allow splitting the total solution into sub-steps to solve for each of the variables first. Each of the segregated steps, uses a parallel sparse direct linear solver called MUMPS (MUltifrontal Massively Parallel sparse direct Solver) that works on general systems on the form of:

$$\mathbf{Ax} = \mathbf{b} \tag{18}$$

The termination of the segregated step was based on the estimated error, so that it terminates if, for all the groups j, the error estimate is smaller than the corresponding tolerance, i.e.:

$$\text{error}_{j,k} < \text{tol}_j \tag{19}$$

where k is the iteration number. A backward differentiation formulas (BDF) are used for time stepping, and the steps taken by the solver are free to be determined by the solver. The BDF takes the general form [1]:

$$\sum_{i=0}^{s} \alpha_i y_{n+i} = h\beta f(t_{n+s},\ y_{n+s}) \tag{20}$$

where h denotes the step size, and the coefficient α and β were chosen by the program. The maximum and minimum orders of the BDF method were set to 2 and 1, respectively. The total number of degrees of freedom solved for in the

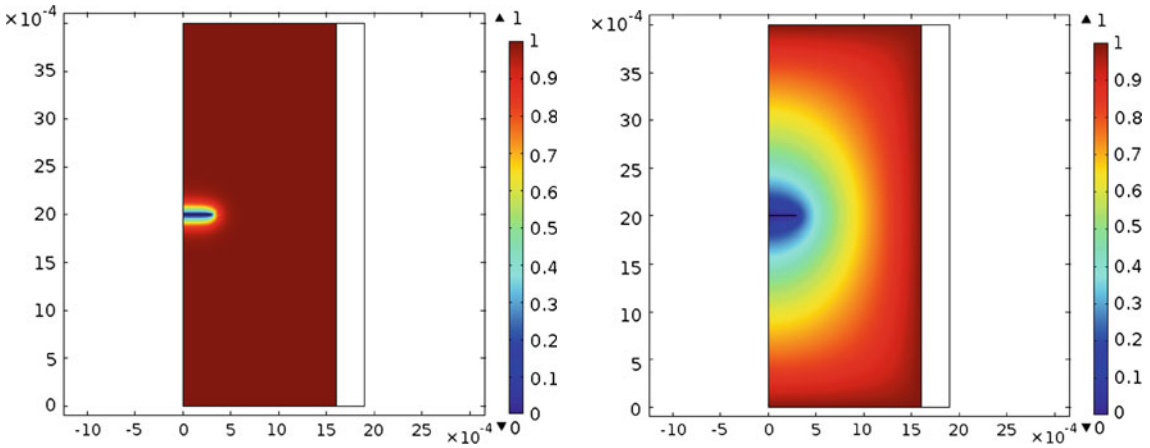

(a) t=0 s **(b)** t=0.1 s

Fig. 5 Distribution of the phase-field parameter ϕ, $Q = 1\,MJ/m^2$

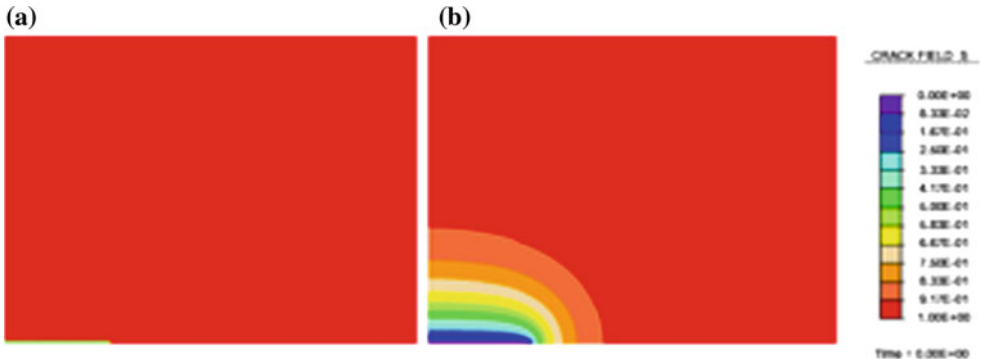

Fig. 6 Distribution of the phase-field parameter s [10]

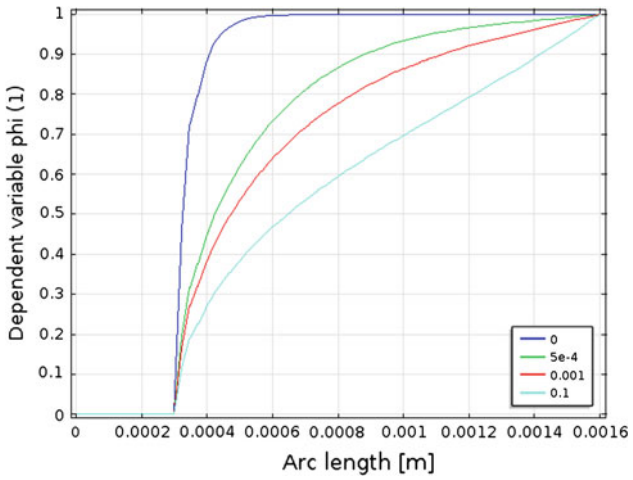

Fig. 7 Snapshots of the values of ϕ for $Q = 1\,\mathrm{MJ/m^2}$

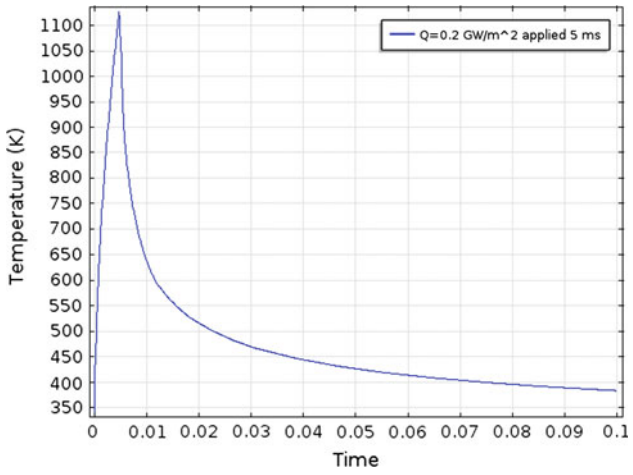

Fig. 8 Evolution of surface temperature for $Q = 1\,\mathrm{MJ/m^2}$

model are 157,451 degrees of freedom. Figure 4 shows the evolution of the reciprocal of the step size as a measure of the convergence of the solution.

The initial and final distribution of ϕ in the material are shown in Fig. 5a, and b, respectively. These results are similar

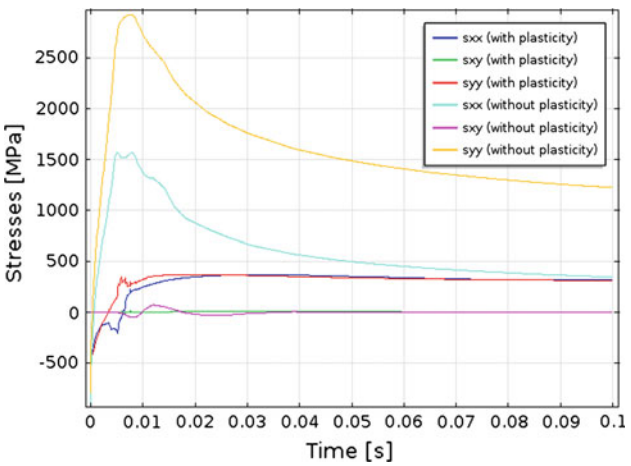

Fig. 9 Stresses at a point near the crack tip with and without the effect of plasticity

to the results obtained by Kuhn in [10] under pure mechanical loading (Fig. 6). Another way to visualize the opening of the crack, is to look at the values of the order parameter ϕ across the material, at different time instances. This is given in Fig. 7. For the heat flux and duration used in this simulation, the temperature reached a maximum value of 1,100 K (Fig. 8) at the surface of the tungsten material.

In Fig. 9, normal and shear stresses are plotted at a point near the crack tip, where plastic deformation is also accounted for. Several observations can be deduced from the graph. First, the value of the stresses when plasticity was included is much lower than its counterpart without the plasticity. Second, after some initial fluctuations, with the plasticity added, the stresses reach a plateau that seems to stay at a constant value. This plateau is the residual stresses that remain in the material, even after the removal of the applied load (switching-off the heat flux in this case). The same argument is not true in the case when plasticity was not included, as the stresses are decreasing and will asymptotically reach zero. Finally, The distribution of stresses and strains in tungsten are given in Fig. 10.

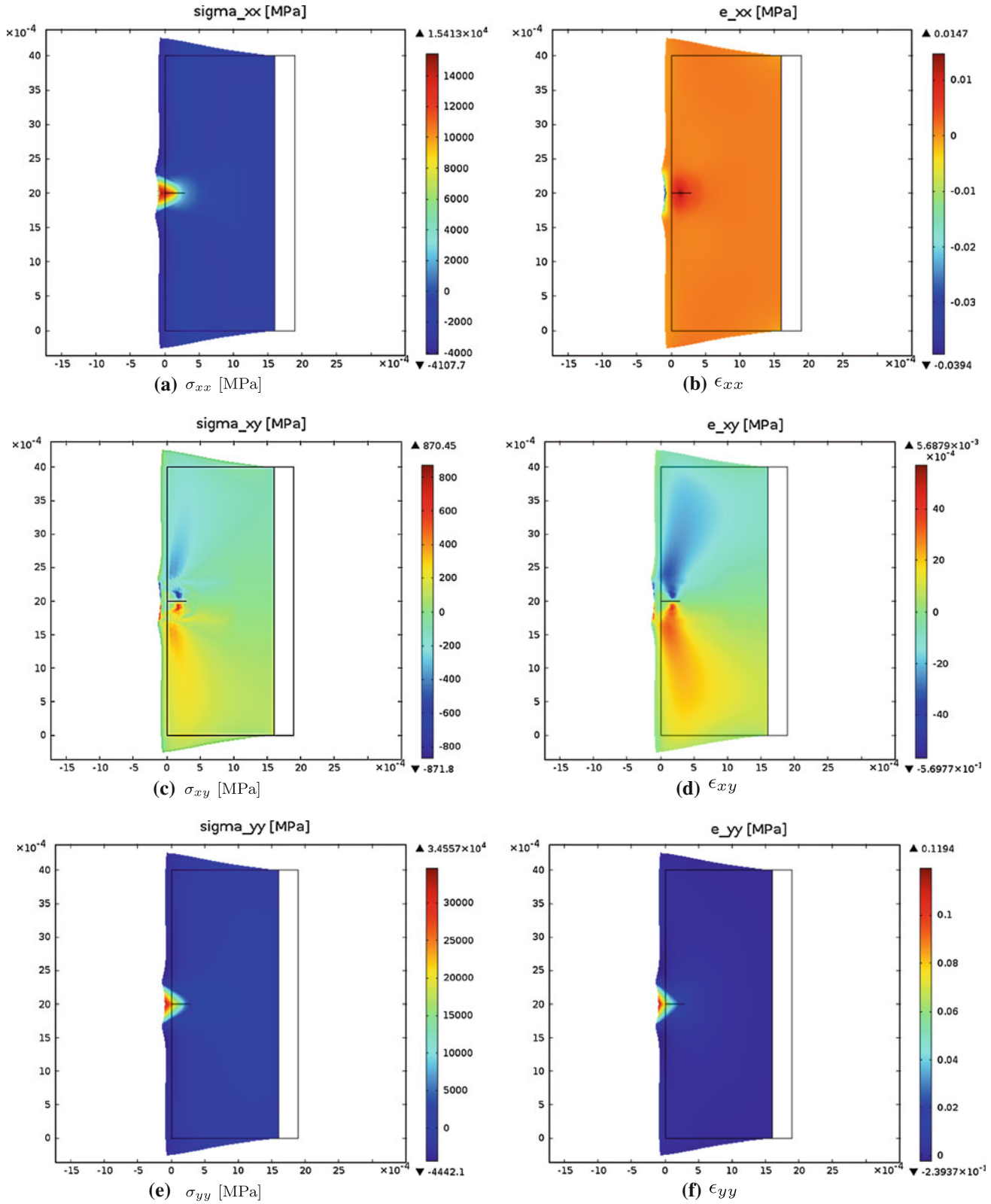

(a) σ_{xx} [MPa] **(b)** ϵ_{xx}

(c) σ_{xy} [MPa] **(d)** ϵ_{xy}

(e) σ_{yy} [MPa] **(f)** ϵ_{yy}

Fig. 10 Stress and strain distribution in the deformed tungsten, $Q = 1\,\mathrm{MJ/m^2}$ at $t = 1\,\mathrm{ms}$

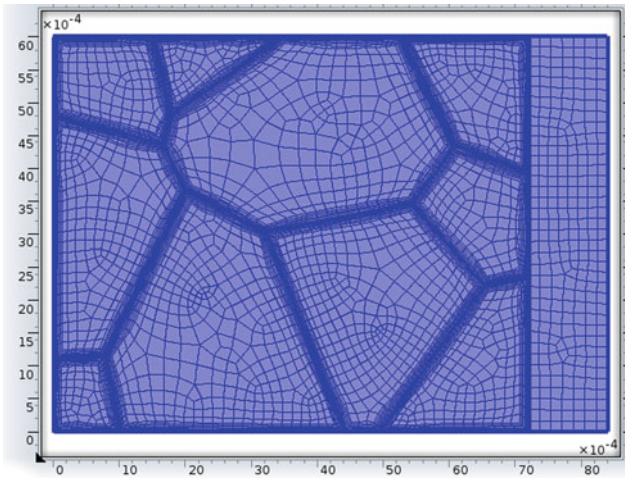

Fig. 11 Mixed quadrilateral and boundary element meshes for the tungsten material

4 Fracture damage of polycrystalline tungsten under thermal shock

The previous multiphysics model was implemented on polycrystalline tungsten to study the effect of the thermal loads on inter-granular crack formation. The modeled geometry was a two-dimensional (7 mm × 6 mm) block. The method of Voronoi diagrams was used to divide the geometry into a random number of grains with different sizes and orientations. Figure 11 shows the mixed quadrilateral and boundary layer meshes used in the simulation. The constitutive and physical parameters for tungsten were all chosen as a function of temperature, to allow them to vary with the change in temperature. The boundary conditions were similar to the case of the slap but with different values for the heat fluxes used. The initial conditions were set similar to the slap case,

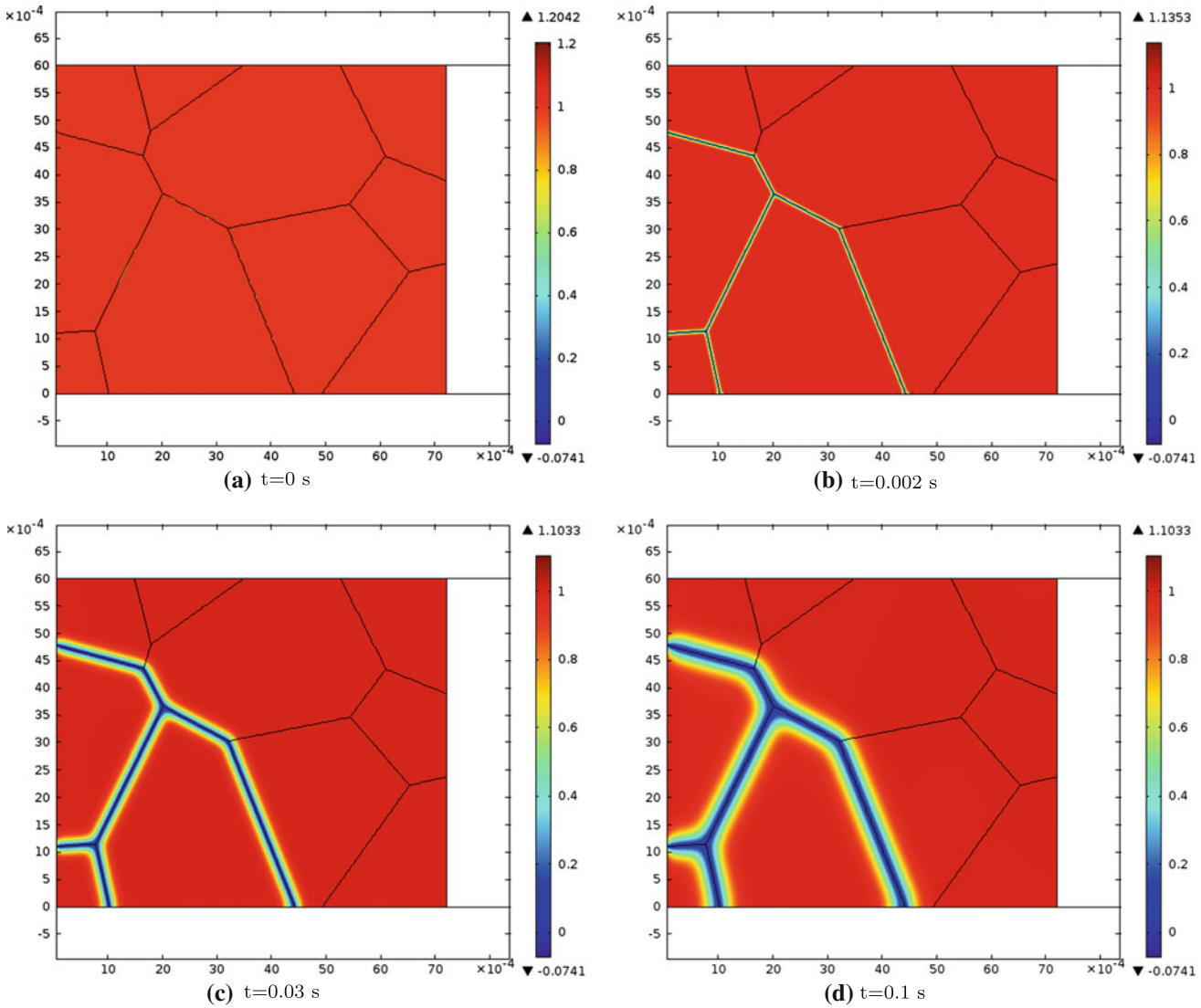

Fig. 12 Snapshots of the distribution of the phase-field parameter ϕ, $Q = 1\,\mathrm{MJ/m^2}$

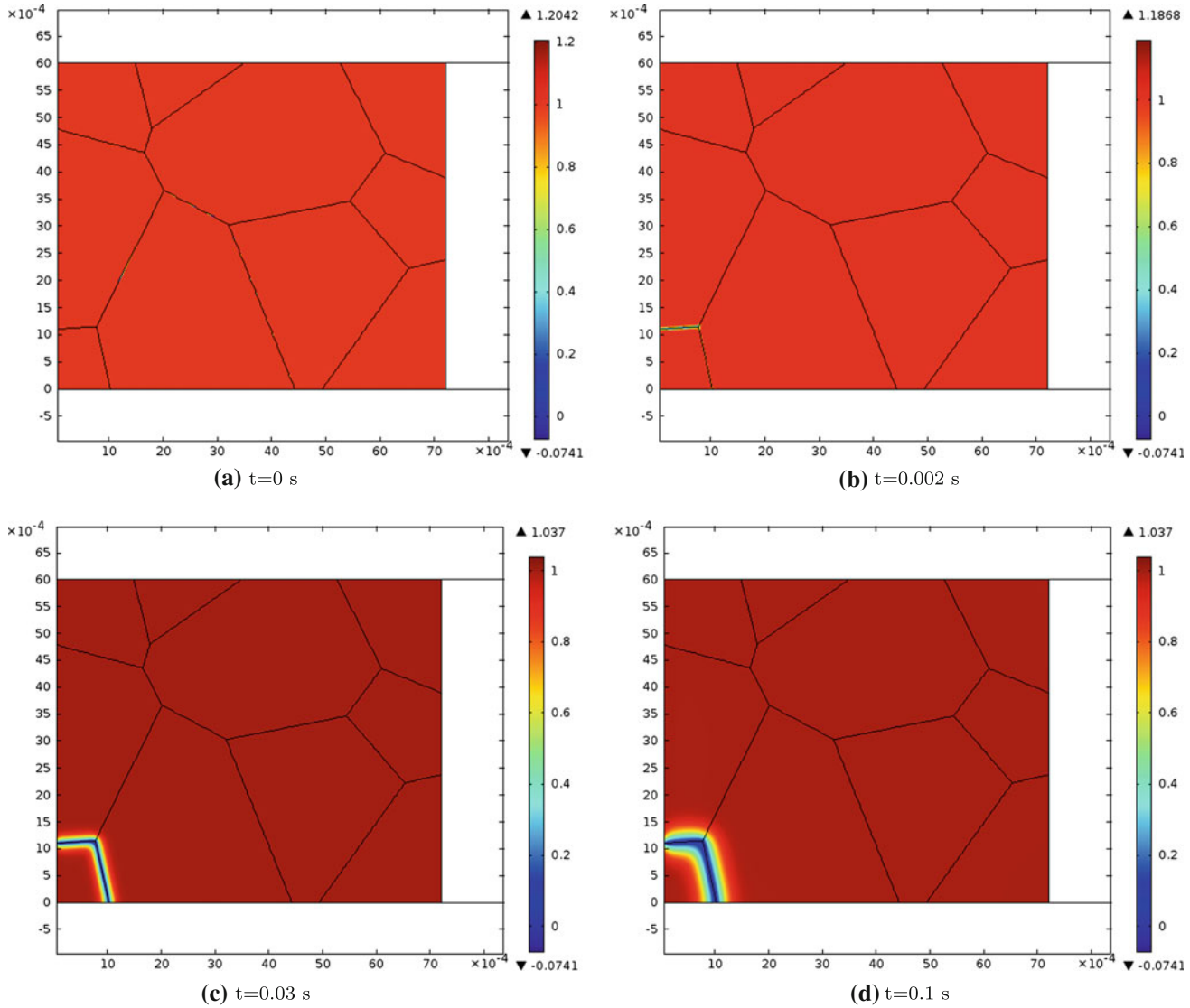

Fig. 13 Snapshots of the distribution of the phase-field parameter ϕ, $Q = 0.1\,\mathrm{MJ/m^2}$

except that we added additional constraints on grain boundaries to allow for nucleation of new cracks. These constraints are based upon the Griffith criterion which states that crack initiation will take place inside a material when the energy release rate reaches a value greater than the material surface energy. The Griffith criterion is expressed as [6]:

$$G \geq 2\gamma_c \tag{21}$$

The surface energy for tungsten used in this study is 2.5 N/m [7]. Two cases with different heat fluxes of 1 and $0.1\,\mathrm{GW/m^2}$, both applied for a duration of 1 ms, were studied. These selected values resemble conditions expected in ITER during ELM transient loads. Figure 12 shows snapshots of the distribution of the phase-field parameter ϕ for the case when $Q = 1\,\mathrm{MJ/m^2}$. The snapshots show the progression of the opening of cracks. In that case, cracks have propagated to deep distances inside the material. This is not the case when the heat load was $0.1\,\mathrm{MJ/m^2}$, as can be seen in Fig. 13 that cracks didn't propagate at the high depth inside the material. The peak values of temperature for the two pervious cases are different as shown in Fig. 14. For the severe transient case, the temperature reached a value of 2,200 K. This temperature is much higher than the peak value reached in the case of the slap, even though both cases were subjected to same heat load. However, since the duration of the heat flux was different, and the heat flux value was also different, the peak values ended up being not the same, even for the same heat load. This shows that the duration of the heat flux can play a role in determining the temperature profile inside the material, which in turn affects the damage. The difference in the depth of cracks is due to the heat flux and the temperature gradient developed inside the material. Figure

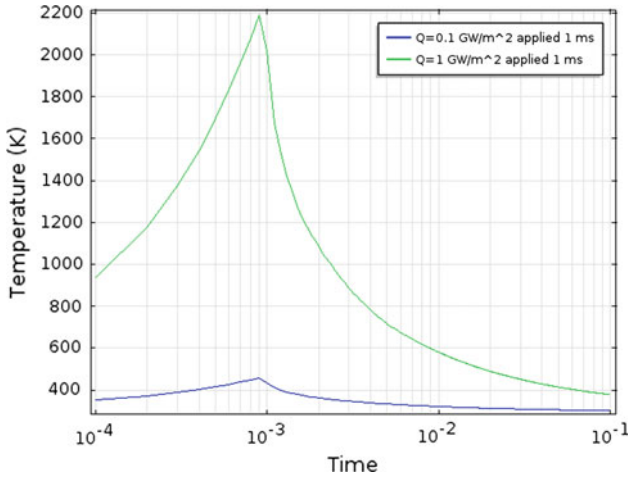

Fig. 14 Evolution of surface temperature for two transient heat loads typical of ELMS in fusion energy devices

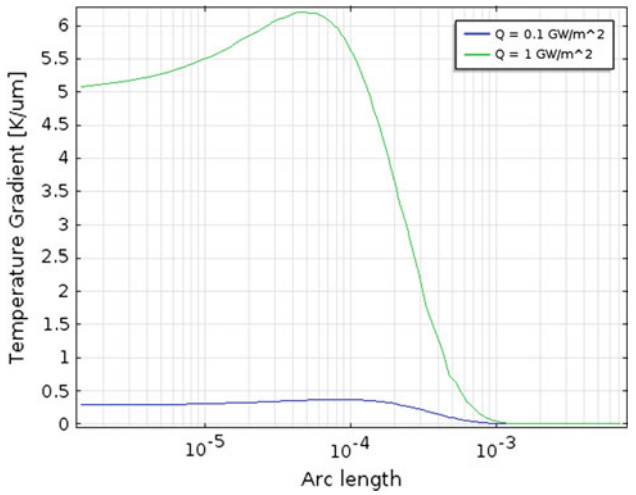

Fig. 15 The temperature gradient (K/μm) for different heat loads at $t=1$ ms

15 shows that in the case of higher heat load, the temperature gradient reaches a value around 6 K/μm, while in the other case the temperature gradient was 0.25 K/μm.

5 Conclusions

Transient heat loads in fusion and space electric propulsion systems are characterized with large values of energies applied for a short duration. Surface and inter-granular cracks appear as the outcome of these thermal shock events. We developed here a mathematical model based on the method of phase-field to study crack propagation and nucleation under these severe operating conditions similar to the ones expected in ITER. The model combines thermo-elasto-plasticity, a crack damage criterion, and thermal conduction, and was developed and implemented within the finite element framework.

First, a two-dimensional block with an initial crack was studied to validate the model. A heat load of 1 MJ/m^2 that was applied for 5 ms was studied. The results showed different aspects of the model, such as the effect of different parameters on the values of ϕ, and the crack profile for different time instances. Some of the results were directly compared to a similar model found in literature. The model also showed that residual stresses remain present in the material. This may help to formulate the design rules for future fusion reactors.

Next, the model was implemented on a polycrystalline tungsten, with the possibility of the nucleation of new cracks. The Griffith energy criterion was employed for determining crack initiation. Two heat loads of 1 and 0.1 MJ/m^2, both applied for 1 ms, were tested. The results showed a difference between crack propagation depth for the two cases. This difference is explained by looking at the difference in the temperature gradient that was developed in the material for the two cases. When the temperature gradient in tungsten reached a value of 6 K/μm, cracks propagated to deeper distances from the surface as compared to a value of 0.25 K/μm. It was also concluded from the simulations that the temperature has a clear effect at, and close to the surface of the material on the crack opening displacement. Also two heat loads can have different effects on the material, if they were applied for different time periods, such that their heat fluxes are different. In general, the results are found to be in good agreement with the observed experiments, e.g. [4,14], and the developed model opens the door for more complex studies and analyses.

Acknowledgements This research is supported by the Department of Energy, Office of Fusion Energy Sciences, grant number DE-FG02-03ER54078, and also by the Air Force Office of Scientific Research (AFOSR), grant number FA9550-11-1-0282 at UCLA.

References

1. Ascher UM, Petzold LR (1998) Computer methods for ordinary differential equations and differential-algebraic equations. SIAM, Philadelphia
2. Bazylev B, Janeschitz G, Landman I, Pestchanyi S (2005) Erosion of tungsten armor after multiple intense transient events in ITER. J Nucl Mater 337–339:766–770
3. Corson F, Adda-Bedia M, Henry H, Katzav E (2009) Thermal fracture as a framework for quasi-static crack propagation. Int J Fract 158:1–14
4. Garkusha IE, Bandura AN, von Byrka O, von Chebotarev V, Landman I, von Makhlaj A, Pestchanyi S, von Tereshin I (2009) Damage to preheated tungsten targets after multiple plasma impacts simulating ITER ELMs. J Nucl Mater 386–388(C):127–131
5. Goebel DM, Katz I (2008) Fundamentals of electric propulsion: ion and Hall thrusters (JPL space science and technology series) 1st edn. Wiley, New York

6. Griffith A (1921) The phenomena of rupture and flow in solids. Philos Trans R Soc Lond 221:163–198
7. Hodkin E, Nicholas M, Poole D (1970) Surface energies of solid molybdenum, niobium, tantalum and tungsten. J Less-Common Met 20(2):93–103
8. Kachanov LM (2004) Fundamentals of the theory of plasticity. Courier Dover Publications, New York
9. Karma A, Kessler D, Levine H (2001) Phase-field model of mode III dynamic fracture. Phys Rev Lett 87(4):1–4
10. Kuhn C (2010) ScienceDirect—engineering fracture mechanics: a continuum phase field model for fracture. Eng Fract Mech 77:3625–3634
11. Lassila DH, Gray GTIII (1994) Ductile-brittle transition behavior of tungsten under shock loading. J Phys IV 04(C8):C8-349–C8-354
12. Leonard A, Herrmann A, Itami K, Lingertat J, Loarte A, Osborne T, Suttrop W (1999) The impact of ELMs on the ITER divertor. In: Journal of nuclear materials. Gen Atom Co, San Diego, pp 109–117
13. Miehe C, Hofacker M, Welschinger F (2010) A phase field model for rate-independent crack propagation: robust algorithmic implementation based on operator splits. Comput Methods Appl Mech Eng 199:2765–2778
14. Pestchanyi S, Garkusha I, Landman I (2010) Simulation of tungsten armour cracking due to small ELMs in ITER. Fusion Eng Des 85:1–5
15. Provatas N, Elder K (2011) Phase-field methods in materials science and engineering. Wiley-VCH, Weinheim
16. Spatschek R, Brener E, Karma A (2010) Phase field modeling of crack propagation. Philos Mas 91:75–95
17. Zhitlukhin A, Klimov N, Landman I, Linke J, Loarte A, Merola M, Podkovyrov V, Federici G, Bazylev B, Pestchanyi S (2007) Effects of ELMs on ITER divertor armour materials. J Nucl Mater 363–365:301–307